



Self-Referential Plasmonic Refractive Index Sensor by Square Hole Array and Gold Film Coupling Structure

Xijun Rao¹ · Huirong Zhu¹ · Xiangxian Wang¹ · Yizhen Chen¹ · Yunping Qi² · Hua Yang¹

Received: 4 June 2024 / Accepted: 3 July 2024

© The Author(s), under exclusive licence to Springer Science+Business Media, LLC, part of Springer Nature 2024

Abstract

A surface plasmonic refractive index (RI) sensor is proposed based on a square hole array and gold film coupling structure. This sensor enables high-sensitivity sensing with self-reference characteristics in gas and liquid environments. The reflectance spectrum and electric fields are calculated using a finite-difference time-domain (FDTD) method. Meanwhile, the cases of rotating square-hole arrays and changing the incident light of the polarization direction are discussed, respectively. The results show that the varying polarization direction of the incident light does not affect the reflectance spectrum of the composite structure. Rotating the array of square holes further enhances the signal strength of the resonance modes excited by the proposed sensor. The sensor has two resonance modes with different functions: one for self-reference and the other for sensing. In the sensing mode, the sensor sensitivity is 1037 and 1063 nm/RIU in gas and liquid environments, respectively; whereas in self-reference mode, the sensitivity decreases to 0 and 21 nm/RIU in gas and liquid environments, respectively. The sensor has a maximum figure of merit (FOM) of 103 RIU⁻¹. These characteristics realize a highly sensitive sensors with a high FOM and self-reference capabilities, which are advantageous for bioassay detection applications.

Keywords Surface plasmon · Nano-square hole array · Refractive index sensing · Self-reference

Introduction

Surface plasmon resonance (SPR) sensors are gaining increased attention in the field of optical sensing owing to their high sensitivity and label-free detection capabilities [1]. The unique optical properties of SPR enable the development of many nanodevices, such as optical switches [2, 3], meta-lens [4–6], sensors [7–11], surface-enhanced raman scattering [12, 13], lithography [14, 15], and perfect absorber [16, 17]. SPR sensors can overcome the diffraction limit and achieve higher precision detection than traditional optical sensors. Additionally, SPR is sensitive to changes in the refractive index (RI) of the material in the field-enhancement region. The RI of the surrounding medium, which

affects the propagation of surface plasmons, can be accurately measured by analyzing the movement of the resonance angle [18] or wavelength [19, 20]. This property makes SPR sensors highly suitable for a wide range of applications, such as biomedical research [10, 21], environmental monitoring [22], food safety [23], and pharmaceutical analysis [24, 25]. Additionally, RI sensors have been widely studied for detecting trace substances, amongst which RI sensors based on SPR with self-reference characteristics have the broadest application. Refractive index sensors based on SPR mainly include prism composite structures [26], grating composite structures [27–29] and metal-insulator-metal (MIM) waveguide structures [30–34]. Among them, the prism composite structure has the disadvantage of being large and unfavorable for integration, while the MIM waveguide structure is unfavorable for realizing self-reference characteristics [35, 36]. The grating composite structure has the advantages of integrability and the possibility of self-reference.

Self-reference is a unique characteristic that can realize a reference comparison in a system, thereby significantly reducing the interference of external factors on the system [26, 37–39]. Therefore, numerous research has focused on the design and preparation of SPR sensors with high

✉ Xiangxian Wang
wangxx869@lut.edu.cn

✉ Yizhen Chen
Chenyiz@lut.edu.cn

¹ School of Science, Lanzhou University of Technology, Lanzhou 730050, China

² College of Physics and Electronic Engineering, Northwest Normal University, Lanzhou 730070, China

sensitivity and self-reference characteristics. Maji et al. proposed a self-referential hybrid Tamm plasmon polariton sensor that achieved a 200 nm/refractive index unit (RIU) sensitivity for sensing in liquid environments [21]. Wang et al. proposed a composite structure of nano-elliptical cylindrical arrays with gold films that can excite magnetic plasmon polariton (MPP) modes and localized surface plasmon (LSP) modes. The MPP mode and LSP mode achieved detection with a sensitivity of 52.09 nm/RIU and 522.76 nm/RIU for analytes ($n = 1.0\text{--}1.6$) [40]. Sun et al. proposed a multilayer dielectric nano-disk array with gold thin-film composite structure sensor to obtain the sensitivity and FOM of the sensing channel at 672 nm/RIU and 1050 RIU⁻¹ in the analyte RI range of 1.33–1.38, respectively. The sensitivity of the reference mode was 46 nm/RIU [41]. These systems benefit from self-referencing as the sensitivity of the referencing channel is extremely low. However, the sensing channel is still limited by either a low sensitivity, low FOM, or a small detection range of the RI of the analyte.

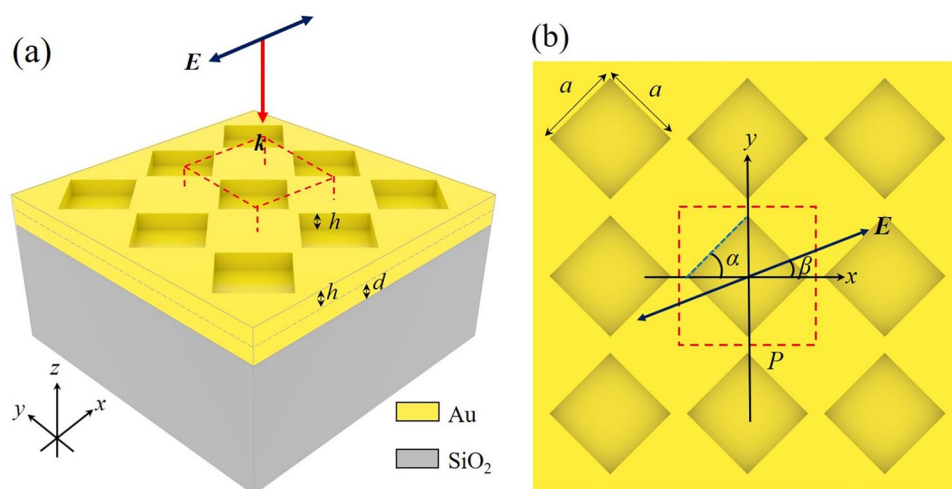
To address these limitations, we propose a plasmonic RI sensor based on a square hole array and a gold film coupling structure. This design provides a self-reference characteristic with high anti-interference and improves sensitivity. The sensor has two resonance modes with different functions: one for self-reference (propagating along the interface between the gold film and the silicon dioxide substrate) and the other for sensing (propagating along the interface between gold nano-square hole arrays and analyte). The nano-square hole and gold film composite structure has a wider sensing range to detect gas and liquid analytes than most other systems discussed in the literature. Moreover, the rotating square aperture arrays and the rotation of the polarization direction of the incident light are discussed. Rotating the direction of the square hole array is beneficial for enhancing the signal intensities of the reference and sensing channels. Rotating the polarization direction of the incident

light had no effect on the reflection spectra that is excited by the composite structure, indicating that the composite structure had little restraint on the polarization direction of the incident light. Moreover, the simple design of the sensor structure facilitated large-area processing.

Structure Design and Theoretical Foundations

The three-dimensional (3D) schematic and planar projection of the nano-square hole array and gold film composite structure are shown in Fig. 1. The composite structure mainly consists of a silicon dioxide substrate, gold film, and gold square hole arrays. The analytes were placed above the nano-square hole and gold film composite structure. The structural parameters of the sensor include the square hole length a , the depth h , the simulation period P , the gold film thickness d , the angle α between the length of the square hole (labeled by the blue dotted line in Fig. 1(b)) and the x -axis, and the angle β between the direction of polarization of the incident light and the x -axis. The reflectance spectrum and electric field distributions of the composite structure were simulated using the finite-difference time-domain (FDTD) method. The schematic x - y plane of the composite structure is shown in Fig. 1(b), where $z = 20$ nm is the plane of the lower surface of the gold film. In the simulation, the mesh size was set to $8 \times 8 \times 8$ nm, the number of monitoring points was set to 10000, the incident light was a plane wave with the initial polarization along x -direction. The red dotted box represents the selected simulation unit. The x - and y -directions were subject to periodic boundary conditions, and the z -direction used a perfectly matched layer (PML). The main operational principle is as follows: the square hole array acts as a two-dimensional (2D) grating for optical momentum compensation to excite the SPR and the position of the field enhancement is regulated in the square hole. This enables the

Fig. 1 (a) Three-dimensional schematic and (b) planar projection of the square hole array gold film coupling structure



excitation of two independent propagating surface plasmon resonances (PSPRs) at the top and bottom of the gold film, facilitating self-referential sensing for detecting the RI of the analyte. The steps to fabricate of this sensor are simple, and large-scale fabrication can be achieved through electron beam evaporation and lithography. First, a gold film of thickness d is deposited on the substrate surface by electron beam evaporation. Then, negative photoresist is spin-coated on the gold film surface. Subsequently, the complementary structure of the proposed composite structure is etched through exposure and development steps. Next, a gold layer of thickness h is deposited on the surface of the complementary structure using electron beam evaporation. Finally, the proposed composite structure is obtained by removing the photoresist. In practical refractive index sensing detection: First, the analyte is placed on the upper surface of the composite structure. Then, for detection, the incident light is irradiated perpendicularly on the upper surface of the composite structure through the beam splitter. Finally, the reflected light from the surface of the composite structure is reflected through the beam splitter and measured by a spectrometer [19].

The square-hole array was used as a 2D grating to satisfy the wave vector matching condition for exciting the SPR as follows:

$$k_{light} + k_{grating} = k_{SPR} \tag{1}$$

where k_{light} , $k_{grating}$, and k_{SPR} correspond to the wave vector of the incident light, grating compensation and excited SPR, respectively.

Two PSPR modes were excited in this study: one that occurred at the gold film-analyte interface and the other at the gold film-substrate interface. The SPR is mainly excited at the interface between the metal and the medium. The dielectric constant of the metal is closely related to the wavelength of the incident light. This relationship can be accurately described using the Drude model [9]. Therefore, the PSPR mode at the gold film-analyte interface follows the relationship:

$$k_{SPR} = k_0 n_a \sin\theta + 2\pi \frac{\sqrt{n^2 + m^2}}{P} = \frac{2\pi}{\lambda_0} \sqrt{\frac{\text{Re}(\epsilon_m) \times n_a^2}{\text{Re}(\epsilon_m) + n_a^2}} \tag{2}$$

where θ is the incident angle of incident light, n and m are diffraction orders, the simulation period (P), and ϵ_m is the dielectric constant of the metal. Equation (2) can be further simplified as follows

$$\lambda_{res} = \frac{P}{\sqrt{n^2 + m^2}} \sqrt{\frac{\text{Re}(\epsilon_m) \times n_a^2}{\text{Re}(\epsilon_m) + n_a^2}} \tag{3}$$

where λ_{res} is the resonance wavelength of PSPR mode. According to Eq. (3), the resonance wavelength of the PSPR can be calculated. The resonance wavelength of PSPR is

tuned by the simulation period (P), the dielectric constant of the metal (ϵ_m), the diffraction order (n and m), and the RI of the analyte (n_a), but is insensitive to the size of the metal nanoparticles. Based on this principle, the reliability of the PSPR mode simulations can be accurately assessed.

The field enhancement region of the PSPR mode propagating along the undersurface of the gold film is the substrate environment. Therefore, Eq. (3) is modified to establish the following relationship:

$$\lambda'_{res} = \frac{P}{\sqrt{(n')^2 + (m')^2}} \sqrt{\frac{\text{Re}(\epsilon_m) \times n_s^2}{\text{Re}(\epsilon_m) + n_s^2}} \tag{4}$$

where λ'_{res} represents the resonance wavelength, n' and m' are diffraction orders, and n_s is the RI of the substrate.

Results and Discussion

Figure 2 shows the reflectance spectrum of the proposed sensor in a liquid environment and the electric field distribution for Modes 1 and 2. The results indicate that the sensor operates well in a liquid environment. Here the parameters of the square-hole array composite structure are: $a = 700$ nm, $h = 50$ nm, $d = 30$ nm, $P = 1050$ nm, $\alpha = 45^\circ$ and $\beta = 0^\circ$. The reflectance spectrum in Fig. 2(a), indicates that Modes 1 and 2 are (1, 0)-order PSPR modes propagating along the undersurface of the gold film and the upper surface of the nano-square hole array, respectively. The reflectivity at the resonance wavelength is 0.59 for Mode 1 and 0.02 for Mode 2, which presents low reflectivity with a strong detection signal. Figure 2(b–e) exhibit the electric field distributions of Modes 1 and 2 at RI of 1.33 for the analyte. In Fig. 2(b) and (d), Mode 1 is mainly caused by the PSPR, which occurs at the interface between the gold film and the silicon dioxide substrate, propagates along the bottom surface of the gold film, and continuously decay in the $-z$ -direction. Mode 1 has a strong electric field enhancement effect in the substrate, but not in the analyte environment. Therefore, the results suggest that Mode 1 is insensitive to changes in analyte RI and has a self-referential function. Similarly, the analysis of Fig. 2(c) and (e) shows that Mode 2 is a PSPR that occurs and propagates along the upper surface of the gold nano-square-hole array. The field-enhanced region of Mode 2 occurs mainly in the analyte environments and continuously decays in intensity along the z -direction thereby suggesting that Mode 2 strongly interacts with the analyte environment [42]. This phenomenon indicates that Mode 2 is sensitive to changes in the analyte RI and can be used as a sensing mode. The analysis of the electric field distribution, indicates that the composite structure has self-reference characteristic. Moreover, the sensing performance for the composite structure is discussed in detail later in this paper.

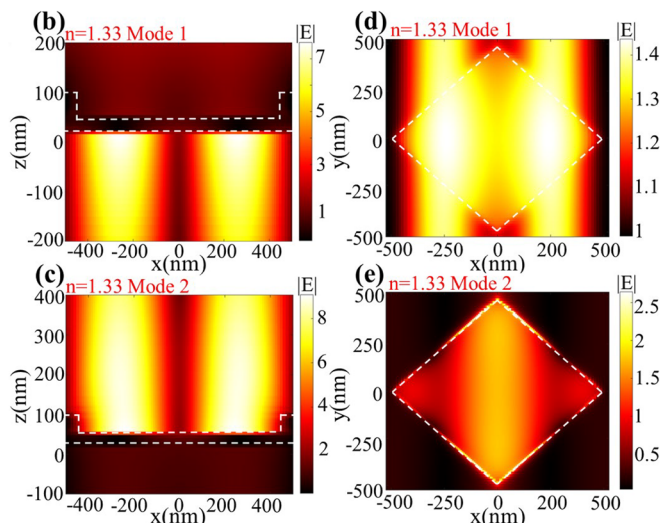
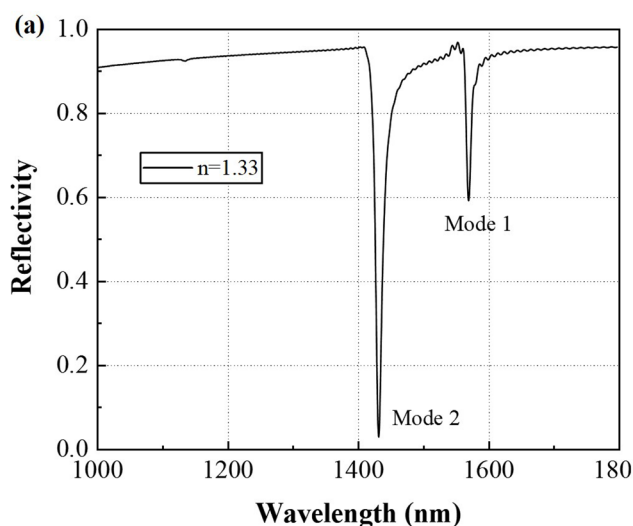


Fig. 2 (a) The reflectance spectrum of the proposed sensor in a liquid environment. (b–e) Electric field distribution at the resonance wavelength. (b) Mode 1 at x - z cross-section with $y=0$ nm, (c) Mode 2 at

x - z cross-section with $y=0$ nm, (d) Mode 1 at x - y cross-section with $z=20$ nm, and (e) Mode 2 at x - y cross-section with $z=50$ nm

The parameters were optimized to further explain the plasmonic effects excited by the sensor. As shown in Fig. 3, the reflectance spectrum of the composite structures was investigated by varying the angle (α) of the square aperture array and the polarization direction of the incident light. In Fig. 3(a), the reflectivity at the dip of Modes 1 and 2 decreases slightly as α changes from 0° to 45° in 5° incremental steps. Here, $\alpha=45^\circ$ was considered as the optical value. In Fig. 3(b), the reflectance spectrum of the sensor is almost constant as β changes. This indicates that the sensor has almost no condition for the polarization direction

of the incident light, which is beneficial for practical applications. Both SPR modes excited by the proposed sensor are PSPR modes, which are insensitive to variations in geometric parameters of individual nano-square holes. Furthermore, based on the arrangement, the proposed structure belongs to a square dot array arrangement. Therefore, for the PSPR mode, from a physical perspective, the change in the polarization direction of the incident light does not affect the reflectance spectrum of the composite structure. The sensing modes are mainly caused by the PSPR modes that propagate along the upper surface of the gold film and

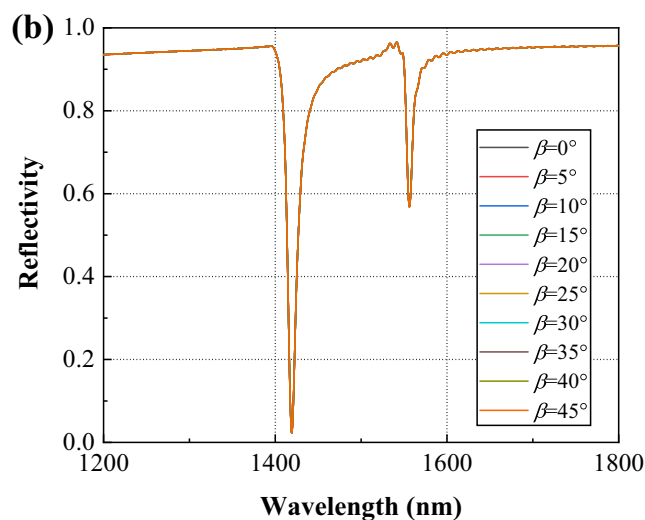
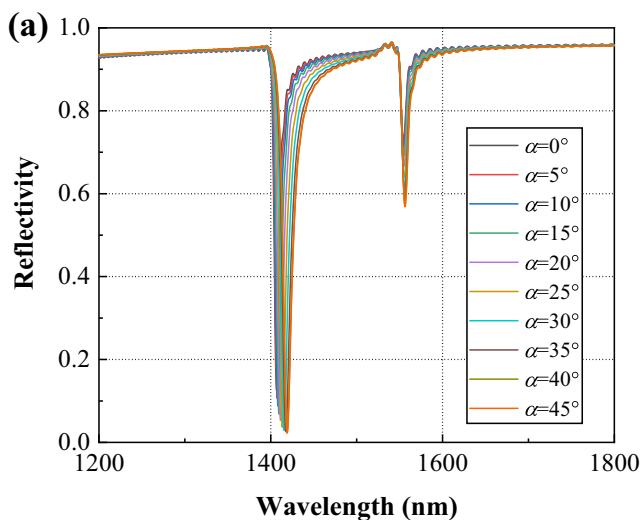


Fig. 3 Reflectance spectrum of composite structures at different values of (a) α and (b) β

decay in the z -direction. The self-reference mode is mainly caused by the PSPR mode that propagates along the lower surface of the gold film and decays in the $-z$ direction. The excitation sensing mode only needs to satisfy the momentum matching condition, and the incident light is directly incident on the upper surface of the composite structure. However, for the self-reference mode, the energy of the incident light needs to penetrate the gold film and be coupled to the lower surface of the gold film. This results in the signal strength of the sensing mode usually higher than that of the self-reference mode [41].

Figure 4 shows the reflectance spectrum of the optimization process for the side length a , depth h of the square holes in the composite structure, and thickness d of the gold film. Figure 4(a) shows that the resonance wavelengths of Modes 1 and 2 remain unchanged as a increases; indicating that the two modes are insensitive to changes in this parameter.

However, significant effect was observed on the signal intensity obtained for $a=700$ nm. In Fig. 4(b), the optimization of the square hole depth was obtained for $h=50$ nm, based on the trade-off between the resonance wavelength of Modes 1 and 2. As Mode 1 was the referencing mode, the resonance wavelength of Mode 2 cannot approach to that of Mode 1. As the RI of the analyte increases, Mode 2 experiences a red-shift. If the resonance of Mode 2 is similar to that of Mode 1, the resonance wavelength of Mode 1 is affected, altering the sensitivity of Mode 1 and limiting the sensing range of the sensor. Therefore, this factor must to be considered during the parameter optimization. At $h=50$ nm, the reflectivity of Mode 2 at the dip was extremely low, at approximately 0. For Fig. 4(c), as d increased, the reflectivity at the resonance wavelength for Mode 1 increased, Mode 2 decreased, and the full width at half maximum (FWHM) for both modes decreased. The resonance wavelengths and

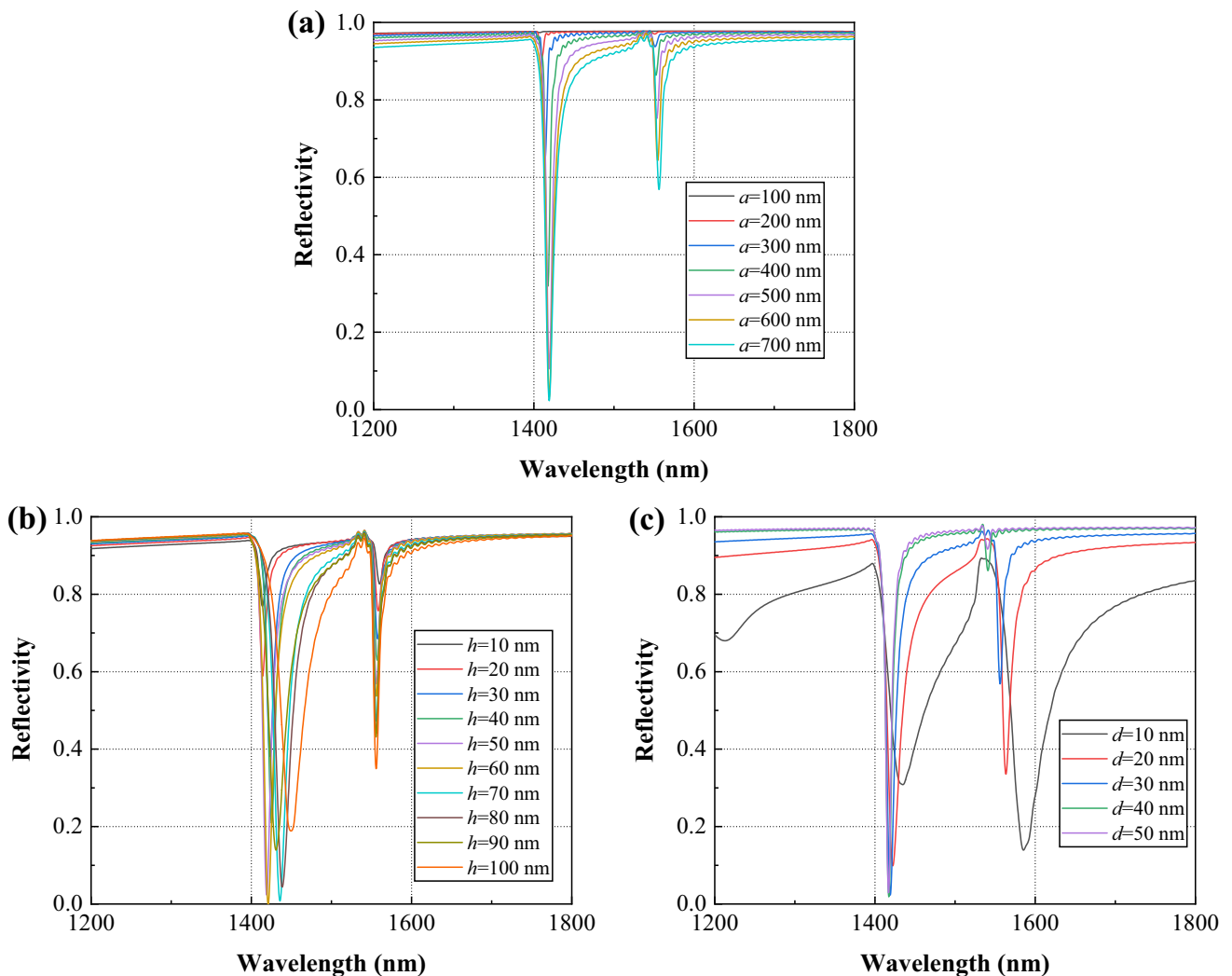


Fig. 4 Reflectance spectrum for different values of (a) the side length a of the square hole, (b) the depth h of the square hole, and (c) the gold film thickness d

FWHM of Modes 1 and 2 were considered, resulting in $d=30$ nm. Figure 4 shows that the resonance wavelengths of Modes 1 and 2 are insensitive to changes in a , h , and d , which further confirms that Modes 1 and 2 are PSPRs. The PSPR is sensitive to changes in the period of the composite structure, whereas the LSPR is sensitive to changes in the size and shape of the nanoparticles [20]. Based on the above analysis of parameter optimization, $a=700$ nm, $h=50$ nm, and $d=30$ nm were obtained.

Next, we examined the effect of the period (P) of the square hole array composite structure on the reflectance spectrum. The theoretical resonance wavelengths of Modes 1 and 2 excited by the composite structure were calculated according to the theoretical equations (Eqs. (3) and (4)). Figure 5(a) shows the reflectance spectrum as the period changes from 1000 to 1250 nm in steps of 50 nm. As the period increases, the resonance wavelengths of Modes 1 and 2 show a significant linear red-shift, which is characteristic of PSPR. In general, the closer the resonance wavelength of the PSPR (as the sensing mode) is to the deep infrared band, the higher the sensitivity of this mode. When $P=1050$ nm, the resonance wavelength of Mode 1 was less than 0.6, which resulted in a trade-off value of $P=1050$ nm.

In addition, the comparison between the simulation results (shown in Fig. 5(a)) and the theoretical analysis results is shown in Fig. 5(b). The results of simulation calculations and theoretical analyses of Modes 1 and 2 were basically fitted, confirming the reliability of sensor. Theoretical analysis implies that Modes 1 and 2 are (1,0) modes ($(n,m)=(n',m')=(1,0)$).

The sensing performance of the proposed sensors and self-referencing characteristics were investigated based on the above analysis. Two crucial-parameters for sensing

performance. One of the parameters are sensitivity (S) and FOM. The expressions for these two parameters are as follows:

$$S = \frac{\Delta\lambda}{\Delta n} \tag{5}$$

$$FOM = \frac{S}{FWHM} \tag{6}$$

where sensitivity (S) quantifies the sensing capability of the sensor, and the FOM quantifies the sensing accuracy.

The sensing performance of the composite structure was investigated based on optimal parameters. Figure 6 shows the sensing performance of the sensor in a liquid environment, where Fig. 6(a) shows the reflectance spectrum of the sensor in a liquid environment, with different colors corresponding to different reflectivity. As the refractive index increased, Modes 1 and 2 exhibited well linear sensitivities, and the resonance wavelengths of the self-reference mode (Mode 1) remained almost constant, whereas that of the sensing mode (Mode 2) is significantly red-shifted. The electric field enhancement region of Mode 1 is located mainly in the substrate environment, while the substrate material remains unchanged. Therefore, the resonance wavelength of Mode 1 remains almost constant when the refractive index of the analyte changes. In contrast, the electric field enhancement region of Mode 2 is located mainly in the analyte environment and is extremely sensitive to changes in the analyte. Mode 2 undergoes a significant linear redshift as the refractive index of the analyte increases. Meanwhile, the FWHMs of Modes 1 and 2 were nearly constant. The FWHMs of Modes 1 and 2 were 8.9 and 12.7 nm in the liquid environment, respectively. Figure 6(b) shows the relationship

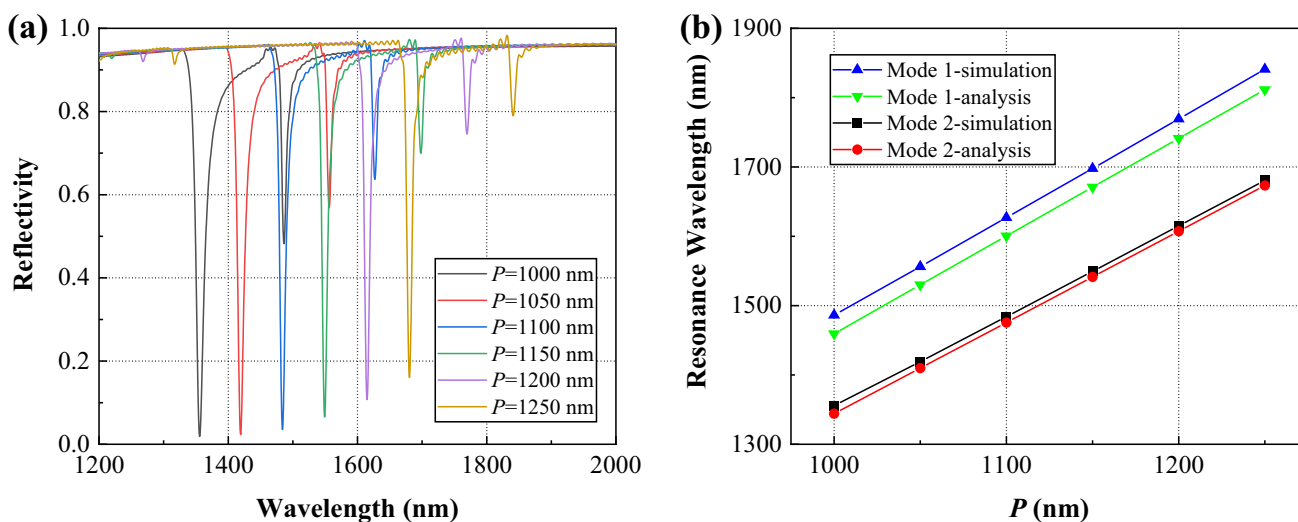
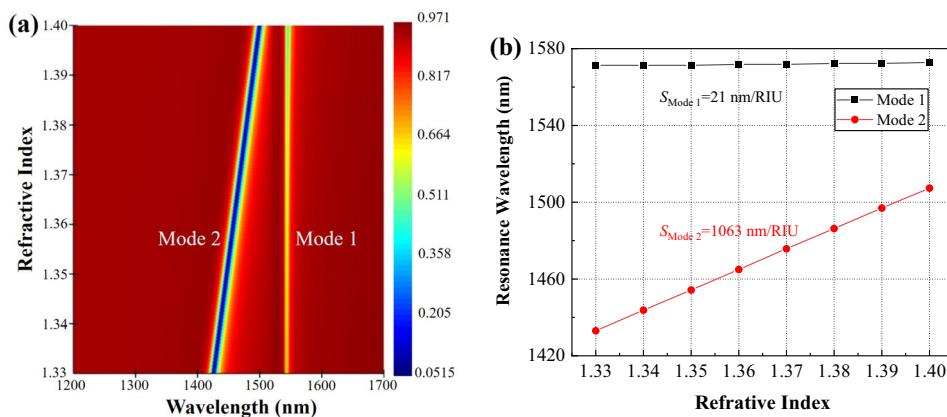


Fig. 5 (a) Reflectance spectrum of the sensor at different simulation periods. (b) Comparison between the simulation and theoretical analysis for PSPRs

Fig. 6 (a) Reflectance spectrum of the proposed sensors in liquid environments. Different colors correspond to different reflectivity. (b) Relationship between resonance wavelength and RI of liquid analytes



between the resonance wavelengths of the two modes and the RI of the different liquid analytes. The sensitivity of Mode 1 in the liquid environment was 21 nm/RIU, whereas the sensitivity and FOM of Mode 2 in the liquid environment were 1063 nm/RIU and 83 RIU⁻¹, respectively. These results demonstrate the high sensitivity and self-reference characteristics of the proposed sensor in liquid environment.

The sensor’s performance in a gas environment was further investigated to broaden its application range. First, Fig. 7 shows the reflectance spectrum of the sensor in a gas environment alongside the electric field distributions for Modes 1 and 2. Identical to the liquid environment, the composite structure can excite two PSPR modes in gas environments. For Fig. 7(b) and (d), Mode 1 is mainly caused by the PSPR, which occurs at the interface between the gold film and the silicon dioxide substrate. This mode, propagates along the underside of the gold film, and decays continuously along the -z-direction. For Fig. 7(c) and (e), Mode 2 is a PSPR that occurs and propagates along the interface between the gold nano-square hole arrays and analyte. The field enhancement region of Mode 2 occurs mainly at the top of the gold nano-square hole array and continuously decays in the z-direction. This demonstrates

that the sensor still exhibits self-reference characteristics in a gas environment.

This analysis provides ample evidence that the sensor exhibits self-reference characteristic. The sensing performance for gas environments is discussed in Fig. 8. Figure 8(a) shows the reflectance spectrum of the sensor in gas environments with different colors corresponding to different reflectivity. Modes 1 and 2 exhibited excellent linear sensitivities with increased RI. Figure 8(b) shows the relationship between the resonance wavelengths of the two modes and the RI of the different gas analytes. Similar to the analysis in Fig. 6, the sensitivity of Mode 1 was 0 nm/RIU. The FWHMs of Modes 1 and 2 were 7.7 nm and 10.3 nm in the gas environment, respectively. The sensitivity and FOM for Mode 2 in the gas environment were 1037 nm/RIU and 103 RIU⁻¹. These results further illustrate that the sensor can perform well in gas and liquid environments.

The performance of the proposed sensor was compared with that of similar sensors previously reported and listed in Table 1 [43–46]. The proposed sensor allows for refractive index sensing with high sensitivity and FOM. In addition, the sensor exhibited excellent self-reference performance. A comprehensive comparison shows that our sensor outperforms the aforementioned studies.

Fig. 7 (a) Reflectance spectrum of the proposed sensors in a gas environment. (b–e) Electric field distribution at the resonance wavelength. (b) Mode 1 at x-z cross-section with y=0 nm, (c) Mode 2 at x-z cross-section with y=0 nm, (d) Mode 1 at x-y cross-section with z=20 nm, and (e) Mode 2 at x-y cross-section with z=50 nm

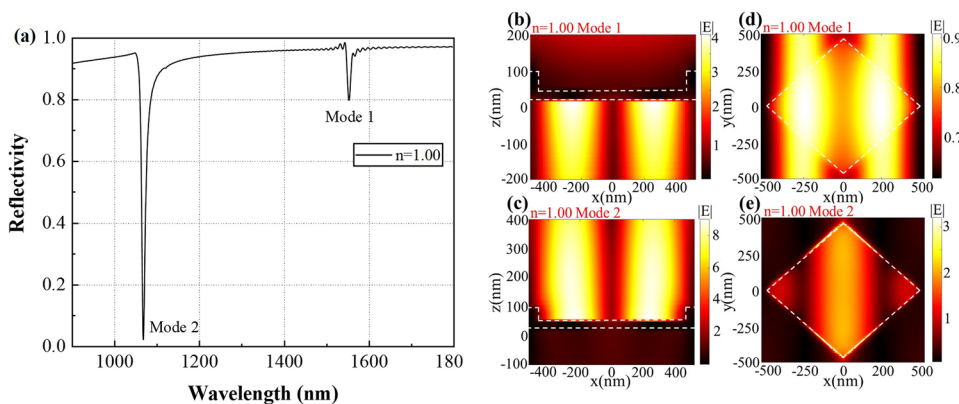


Fig. 8 (a) Reflectance spectrum of the proposed sensors in a gas environment. Different colors correspond to different reflectivity. (b) Relationship between resonance wavelength and RI of gas analytes

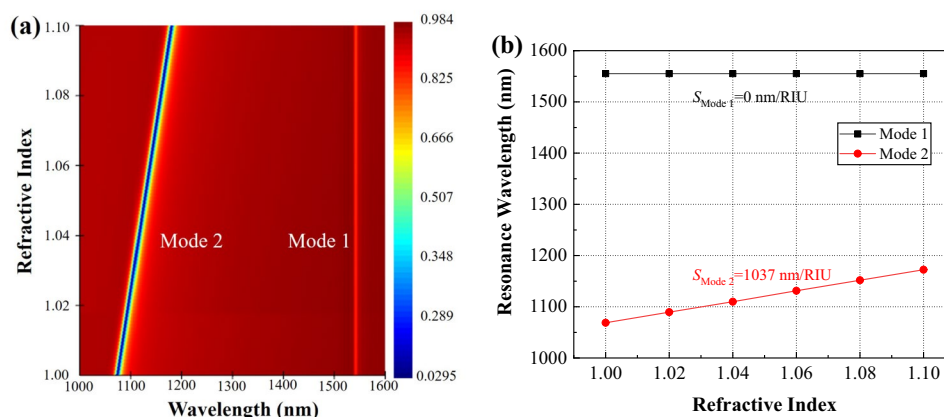


Table 1 Comparison of the performance of the proposed sensor with that of other sensors from literature

Ref.	Coupling structure	Range of Refractive Index (RI)	S (nm/RIU) (sensing & self-referencing)	FWHM (nm)	FOM (RIU ⁻¹)
[43]	silicon nitride gratings and silver thin film composite structures	1.33-1.34	580 & 40	> 10	—
[44]	gold nano-islands	1.0-1.50	212 & 9	~43.2	4.9
[45]	gold grating composite structure	1.33-1.39	720 & —	—	—
[46]	All-dielectric	liquids	760 & 0	0.5	1515
This work	square hole array	1.33-1.40	1063 & 21	12.7	83
This work	square hole array	1.00-1.10	1037 & 0	10.1	103

Conclusion

We propose a self-referential plasmonic sensor based on a square hole array and gold film composite structure. Its sensing performance and field-enhancement phenomena were analyzed using the FDTD method. The sensor can excite the PSPR mode on the top and bottom surfaces of the gold film. The PSPR mode excited on the lower surface of the gold film exhibited excellent self-reference performance, while the PSPR mode excited on the upper surface of the gold nano-square-hole array exhibited excellent sensing performance. The composite structure does not require the specification of the polarization direction of the incident light. At the optimized parameters ($a = 700 \text{ nm}$, $h = 50 \text{ nm}$, $d = 30 \text{ nm}$, and $P = 1050 \text{ nm}$), the sensor achieved high-sensitivity sensing at 1037 and 1063 nm/RIU in gas and liquid environments, respectively. This type of sensor can be widely used for biochemical detection.

Author Contributions Conceptualization: Xijun Rao, Xiangxian Wang, Hua Yang. Methodology: Xijun Rao, Huirong Zhu, Xiangxian Wang. Writing—original draft preparation: Xijun Rao; Writing—review and editing: Huirong Zhu, Xiangxian Wang, Yizhen Chen. Funding acquisition: Xiangxian Wang, Yunping Qi. Project administration: Xiangxian

Wang, Yunping Qi. Software: Xijun Rao, Huirong Zhu, Yizhen Chen, Yunping Qi. Supervision: Xiangxian Wang, Yizhen Chen, Hua Yang.

Funding This work was supported by the National Natural Science Foundation of China (NSFC) (62365012, 62165013).

Data Availability No datasets were generated or analysed during the current study.

Declarations

Competing Interests The authors declare no competing interests.

References

- Rodrigo D, Limaj O, Janner D, Etezadi D, Abajo FJG, Pruneri V, Altug H (2015) Mid-infrared plasmonic biosensing with graphene. *Science* 349(6244):165–168. <https://doi.org/10.1126/science.aab2051>
- Gómez-Díaz JS, Perruisseau-Carrier J (2013) Graphene-based plasmonic switches at near infrared frequencies. *Opt Express* 21(13):15490–15504. <https://doi.org/10.1364/OE.21.015490>
- Ono M, Hata M, Tsunekawa M, Nozaki K, Sumikura H, Chiba H, Notomi M (2020) Ultrafast and energy-efficient all-optical switching with graphene-loaded deep-subwavelength plasmonic waveguides. *Nat Photonics* 14:37–43. <https://doi.org/10.1038/s41566-019-0547-7>

4. Roy T, Rogers ETF, Zheludev NI (2013) Sub-wavelength focusing meta-lens. *Opt Express* 21(6):7577–7582. <https://doi.org/10.1364/OE.21.007577>
5. Prinz E, Spektor G, Hartelt M, Mahro AK, Aeschlimann M, Orenstein M (2021) Functional meta lenses for compound plasmonic vortex field generation and control. *Nano Lett* 21(9):3941–3946. <https://doi.org/10.1021/acs.nanolett.1c00625>
6. Markovich H, Shishkin II, Hendler N, Ginzburg P (2018) Optical manipulation along an optical axis with a polarization sensitive meta-lens. *Nano Lett* 18(8):5024–5029. <https://doi.org/10.1021/acs.nanolett.8b01844>
7. Liu W, Liu C, Wang JX, Lv JW, Lv Y, Yang L, An N, Yi Z, Liu Q, Hu CJ, Chu PK (2023) Surface plasmon resonance sensor composed of microstructured optical fibers for monitoring of external and internal environments in biological and environmental sensing. *Results Phys* 47:106365. <https://doi.org/10.1016/j.rinp.2023.106365>
8. Fu WF, Sun L, Cao HY, Chen L, Zhou M, Shen SY, Zhu YM, Zhuang SL (2023) Qualitative and quantitative recognition of volatile organic compounds in their liquid phase based on terahertz microfluidic EIT meta-sensors. *IEEE Sens J* 23(12):12775–12784. <https://doi.org/10.1109/JSEN.2023.3268167>
9. Chen HW, Wang XX, Zhang J, Rao XJ, Yang H, Qi YP, Tang CJ (2023) Theoretical study of surface plasmonic refractive index sensing based on gold nano-cross array and gold nanofilm. *Phys B* 655:414746. <https://doi.org/10.1016/j.physb.2023.414746>
10. Chou Chao CT, Kooh MRR, Chou Chao YF, Thotagamuge R (2022) Susceptible plasmonic photonic crystal fiber sensor with elliptical air holes and external-flat gold-coated surface. *Photonics* 9:916. <https://doi.org/10.3390/photonics9120916>
11. Lyu JM, Shen AY, Chen L, Zhu YM, Zhuang SL (2023) Frequency selective fingerprint sensor: the Terahertz unity platform for broadband chiral enantiomers multiplexed signals and narrowband molecular AIT enhancement. *PhotonX* 4:28. <https://doi.org/10.1186/s43074-023-00108-1>
12. Wu Y, Wang XX, Wen XL, Zhu JK, Bai XL, Jia TX, Yang H, Zhang LP, Qi YP (2020) Surface-enhanced Raman scattering based on hybrid surface plasmon excited by Au nanodisk and Au film coupling structure. *Phys Lett A* 348(23):126544. <https://doi.org/10.1016/j.physleta.2020.126544>
13. Liu K, Bai YC, Zhang L, Yang ZB, Fan QK, Zheng HQ, Yin YD, Gao CB (2016) Porous Au-Ag nanospheres with high-density and highly accessible hotspots for SERS analysis. *Nano Lett* 16(6):3675–3681. <https://doi.org/10.1021/acs.nanolett.6b00868>
14. Kasani S, Curtin K, Wu N (2019) A review of 2D and 3D plasmonic nanostructure array patterns: fabrication, light management and sensing applications. *Nanophotonics* 8(12):2065–2089. <https://doi.org/10.1515/nanoph-2019-0158>
15. Zhu XL, Czolkos I, Johansson A, Nielsen T, Kristensen A (2021) Master origination by 248 nm DUV lithography for plasmonic color generation. *Appl Phys Lett* 118:141103. <https://doi.org/10.1063/5.0046163>
16. Tang CJ, Nie QM, Cai PG, Liu FX, Gu P, Yan ZD, Huang Z, Zhu MW (2024) Ultra-broadband near-infrared absorption enhancement of monolayer graphene by multiple-resonator approach. *Diam Relat Mater* 141:110607. <https://doi.org/10.1016/j.diamond.2023.110607>
17. Feng SNA, Wang YJ, Fei SR, Yan ZD, Yu LL, Chen J, Tang CJ, Liu FX (2023) Dual ultrahigh-Q Fano resonances of 3D gap metamaterials for slow light from ultraviolet to visible range. *Opt Commun* 549:129811. <https://doi.org/10.1016/j.optcom.2023.129811>
18. Ye HY, Chen CB, Zhou JY, Meng ZM (2021) Sodium-based surface plasmon resonances for high-performance optical sensing in the near infrared. *IEEE J Sel Top Quantum Electron* 27(5):4601308. <https://doi.org/10.1109/JSTQE.2021.3049800>
19. Chou Chao CT, Chen SH, Huang HJ, Kooh MRR, Lim CM, Thotagamuge R, Mahadi AH, Chou Chao YF (2023) Improving temperature-sensing performance of photonic crystal fiber via external metal-coated trapezoidal-shaped surface. *Crystals* 13:813. <https://doi.org/10.3390/cryst13050813>
20. Wang XX, Rao XJ, Zhu JK, Chen YZ, Qi YP, Tang CJ, Yang H (2024) Infrared plasmonic refractive index sensor utilizing 2D grating of nano-bowtie particles for both gas and Liquid. *J Opt* 26:035002. <https://doi.org/10.1088/2040-8986/ad2257>
21. Maji PS, Shukla MK, Das R (2018) Blood component detection based on miniaturized self-referenced hybrid Tamm-plasmon-polariton sensor. *Sens Actuators* 225(1):729–734. <https://doi.org/10.1016/j.snb.2017.08.03>
22. Becerril-Castro IB, Munoz-Munoz F, Castro-Ceseña AB, González AL, Alvarez-Puebla RA, Romo-Herrera JM (2021) Plasmonic foam platforms for air quality monitoring. *Nanoscale* 3:1738–1744. <https://doi.org/10.1039/D0NR07686D>
23. Fang BL, Xu SL, Huang YJ, Su FM, Huang Z, Fang H, Peng J, Xiong YH, Lai WH (2020) Gold nanorods etching-based plasmonic immunoassay for qualitative and quantitative detection of aflatoxin M1 in milk. *Food Chem* 329:127160. <https://doi.org/10.1016/j.foodchem.2020.127160>
24. Alberti G, Zanoni C, Spina S, Magnaghi LR, Biesuz R (2023) Trends in molecularly imprinted polymers (MIPs)-Based plasmonic sensors. *Chemosensors* 11(2):144. <https://doi.org/10.3390/chemosensors11020144>
25. Akgönüllü S, Denizli A (2023) Plasmonic nanosensors for pharmaceutical and biomedical analysis. *J Pharm Biomed Anal* 236:115671. <https://doi.org/10.1016/j.jpba.2023.115671>
26. Zhao ML, Wang JX, Zhang YZ, Ge MF, Zhang PY, Shen J, Li CY (2022) Self-referenced refractive index sensor based on double-dips method with bimetal-dielectric and double-groove grating. *Opt Express* 30(5):8376–8390. <https://doi.org/10.1364/OE.454344>
27. Chou Chao CT, Kooh MRR, Lim CM, Thotagamuge R, Mahadi AH, Chou Chao YF (2023) Visible-range multiple-channel metal-shell rod-shaped narrowband plasmonic metamaterial absorber for refractive index and temperature sensing. *Micromachines* 14:340. <https://doi.org/10.3390/mi14020340>
28. Sabaruddin NR, Tan YM, Chou Chao CT, Kooh MRR, Chou Chao YF (2024) High sensitivity of metasurface-based five-band terahertz absorber. *Plasmonics* 19:481–493. <https://doi.org/10.1007/s11468-023-01989-5>
29. Chou Chao CT, Chen SH, Huang HJ, Chou Chao YF (2023) Near- and mid-infrared quintuple-band plasmonic metamaterial absorber. *Plasmonics* 18:1581–1591. <https://doi.org/10.1007/s11468-023-01881-2>
30. Kazanskiy NL, Butt MA, Khonina SN (2020) Nanodots decorated MIM semi-ring resonator cavity for biochemical sensing applications. *Photonics Nanostruct Fundam Appl* 42:100836. <https://doi.org/10.1016/j.photonics.2020.100836>
31. Pinton N, Grant J, Collins S, Cumming DRS (2018) Exploitation of magnetic dipole resonances in metal-insulator-metal plasmonic nanostructures to selectively filter visible light. *ACS Photonics* 5(4):1250–1261. <https://doi.org/10.1021/acsphotonics.7b00959>
32. Salah HB, Bahri H, Hocini A, Zegaar I, Ingebrandt S, Pachauri V (2022) Design of a plasmonic sensor based on a nanosized structure for biochemical application. *J Phys Conf Ser* 2240:012024. <https://doi.org/10.1088/1742-6596/2240/1/012024>
33. Chou Chao YF, Chou Chao CT, Chiang HP (2020) Ultra-broad bandgap metal-insulator-metal waveguide filter with symmetrical stubs and defects. *Results Phys* 17:103116. <https://doi.org/10.1016/j.rinp.2020.103116>
34. Qu D, Sun Y, Ren Y, Wu QH, Li CL (2024) Research on sensing characteristics of triple independent tuning with high sensitivity

- based on MIM waveguide. *Opt Quant Electron* 56:137. <https://doi.org/10.1007/s11082-023-05706-8>
35. Lai WH, Wen KH, Lin JY, Guo ZC, Hu QY, Fang YH (2018) Plasmonic filter and sensor based on a subwavelength end-coupled hexagonal resonator. *Appl Opt* 57:6369–6374. <https://doi.org/10.1364/AO.57.006369>
 36. Chou Chao CT, Chou Chau YF, Chiang HP (2021) Multiple Fano resonance modes in an ultra-compact plasmonic waveguide-cavity system for sensing applications. *Results Phys* 27:104527. <https://doi.org/10.1016/j.rinp.2021.104527>
 37. Wang H, Cai X, Dai W, Luo J, Rao W, Fu H (2022) A double-layer structure SPR sensor with temperature self-compensation and ultra-wide sensing range for RI detection. *IEEE Sens J* 22(3):2309–2316. <https://doi.org/10.1109/JSEN.2021.3135116>
 38. Wang XX, Zhu JK, Xu YQ, Qi YP, Zhang LP, Yang H, Yi Z (2021) A novel plasmonic refractive index sensor based on gold/silicon complementary grating structure. *Chin Phys B* 30(2):024207. <https://doi.org/10.1088/1674-1056/abd690>
 39. Rao XJ, Wang XX, Chen HW, Chen YZ, Qi YP, Yang H (2024) Highly sensitive self-referential plasmonic sensor based on double-layer nested grating. *Opt Commun* 558:130348. <https://doi.org/10.1016/j.optcom.2024.130348>
 40. Wang ZK, Chen YK, Sun WJ, Li JF, An XY, Shen ZH (2024) A robust on-chip refractive index sensor assisted by magnetic plasmon polaritons. *Opt Mater* 148:114863. <https://doi.org/10.1016/j.optmat.2024.114863>
 41. Sun P, Zhou CH, Jia W, Wang J, Xiang CC, Xie YF, Zhao D (2020) Self-referenced refractive index sensor based on hybrid mode resonances in 2D metal-dielectric grating. *J Phys D: Appl Phys* 53:145101. <https://doi.org/10.1088/1361-6463/ab6624>
 42. Chou Chao YF (2024) Enhancing broadband terahertz absorption via a graphene-based metasurface absorber featuring a rectangular ring and triple crossbars. *Phys Scr* 99:055905. <https://doi.org/10.1088/1402-4896/ad3516>
 43. Abutoama M, Abdulhalim I (2015) Self-referenced biosensor based on thin dielectric grating combined with thin metal film. *Opt Express* 23:28667–28682. <https://doi.org/10.1364/OE.23.028667>
 44. Barrios CA, Mirea T, Represa MH (2023) A self-referenced refractive index sensor based on gold nanoislands. *Sensors* 23(1):66. <https://doi.org/10.3390/s23010066>
 45. Wang YJ, Sun CW, Li HY, Gong QH, Chen JJ (2017) Self-reference plasmonic sensors based on double Fano resonances. *Nanoscale* 9(31):11085–11092. <https://doi.org/10.1039/C7NR04259K>
 46. Sun P, Xie YF, Xiang CC, Wang J, Jia W, Zhou CG (2020) Non-equidistant arrangement in all-dielectric quadrumers and mirror-symmetric one-dimensional photonic crystals hybrid-structure for self-referenced sensing scheme. *J Lightwave Technol* 38(23):6671–6677. <https://doi.org/10.1109/JLT.2020.3013672>

Publisher's Note Springer Nature remains neutral with regard to jurisdictional claims in published maps and institutional affiliations.

Springer Nature or its licensor (e.g. a society or other partner) holds exclusive rights to this article under a publishing agreement with the author(s) or other rightsholder(s); author self-archiving of the accepted manuscript version of this article is solely governed by the terms of such publishing agreement and applicable law.